AN ANALYSIS OF IRAS' SOLAR SYSTEM DUST BANDS

S. F. Dermott, P. D. Nicholson, J. A. Burns,
and J. R. Houck
Center for Radiophysics and Space Research
Cornell University
Ithaca, NY 14853
U.S.A.

ABSTRACT. Measurements of longitudinal variations in the brightness and in the latitude of the solar system dust bands recently discovered by IRAS will determine the orbital elements of the particles involved and may discriminate between cometary and asteroidal models of the origin of these bands. The expected variations for bands of dust particles with common orbital elements and small eccentricity and inclination are calculated as functions of semimajor axis.

1. INTRODUCTION

During its all-sky survey at wavelengths of 12, 25, 60, and 100 μm, the Infrared Astronomical Satellite (IRAS)[1] discovered three narrow bands of warm (165-200K) emission circling the sky at geocentric ecliptic latitudes ~ -10°, 0°, and 10° (Low et al., 1984; Neugebauer et al., 1984). The inferred heliocentric distance of the bands is 2.7 ± 0.5 AU, suggesting an association with the asteroid belt (Low et al., 1984). The symmetry of the bands with respect to the ecliptic suggests that they are caused by at least two sets of particles, each of which has a common inclination and, more or less, uniformly distributed nodal lines. The paired bands then arise because particles in inclined orbits spend a disproportionate amount of time at the extremes of their vertical harmonic oscillations (Low et al., 1984; Dermott et al., 1984).

Following the suggestion of Low et al. (1984) that the bands could be the results of collisions between asteroids, we have shown that the bands may be associated with the principal Hirayama asteroid families, that is, the Koronis, Eos and Themis families (Dermott et al., 1984). The latitudinal distribution of the asteroids in these families nicely matches the IRAS observations, with the Eos family producing the outer

[1]The Infrared Astronomical Satellite was developed and operated by the Netherlands Agency for Aerospace Programs (NIRV), the U.S. National Aeronautics and Space Administration (NASA), and the U.K. Science and Engineering Research Council (SERC).

R. H. Giese and P. Lamy (eds.), Properties and Interactions of Interplanetary Dust, 395–409.

bands, and the Koronis and Themis families accounting for the central band. Furthermore, if we assume that the lower cutoff in the size distribution of asteroidal particles is ~1 mm (Dohnanyi, 1976), then the families could provide the optical depth ($\sim 10^{-8}$) observed by IRAS. Detailed analysis of the structure of the dust bands as revealed by the IRAS data will test the asteroid hypothesis, since measurements can be made that will determine the orbital elements of the dust particles, in particular, their semimajor axes or mean distances. Here, we outline the analysis needed to relate the perturbations of the dust particle orbits by Jupiter, Saturn, and the other planets to the longitudinal variations in brightness and ecliptic latitude that we predict will exist in the IRAS data.

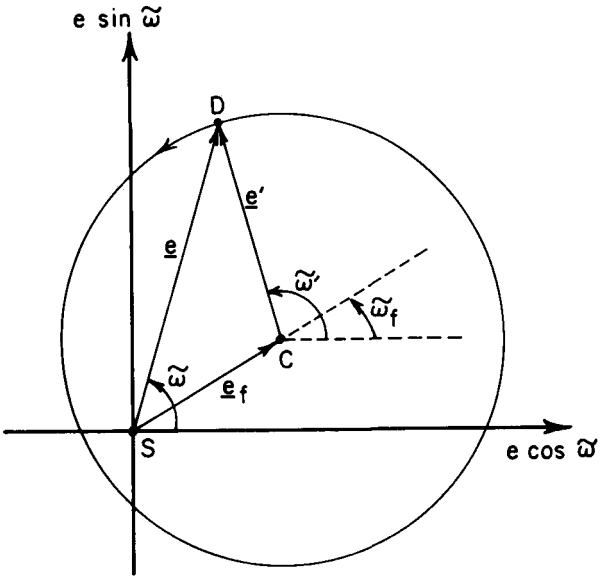

Fig. 1 Vector addition diagram relating the osculating eccentricity $\underline{e}$, the proper eccentricity $\underline{e}'$, the forced eccentricity $\underline{e}_f$ and their corresponding longitudes of pericenter: $\tilde{\omega}$, $\tilde{\omega}'$ and $\tilde{\omega}_f$.

2. SECULAR PERTURBATIONS

Perturbations by Jupiter and, to a lesser extent, Saturn and the other planets result in periodic variations in the eccentricities and the inclinations of asteroidal orbits. If the eccentricity and the inclination are small, then the eccentricity vector can be described as follows:

$$e \sin\tilde{\omega} = e'\sin(\tilde{\omega}_0' + \dot{\tilde{\omega}}'t) + e_f \sin\tilde{\omega}_f, \quad (1)$$

$$e \cos\tilde{\omega} = e'\cos(\tilde{\omega}_0' + \dot{\tilde{\omega}}'t) + e_f \cos\tilde{\omega}_f. \quad (2)$$

https://doi.org/10.1017/S0252921100084980 Published online by Cambridge University Press

(see Fig. 1). Here, $\tilde{\omega}$ is the orbit's longitude of perihelion measured relative to an inertial axis, $\dot{\tilde{\omega}}'$ is the secular apsidal precession rate due to planetary perturbations, and $\tilde{\omega}_f$ is the (slowly varying) forced longitude of perihelion. The constants e' and $\tilde{\omega}_0'$ reflect initial conditions. The inclination vector can be described analogously, in terms of a proper inclination, I', and a forced inclination and nodal longitude, I_f and Ω_f. Proper orbital elements of the Koronis, Eos and Themis Hirayama families are listed in Tables 1 and 2. The forced orbital elements shown in Table 2 were calculated using the theory of Brouwer and van Woerkom (1950) which includes the effects of all the planets except Pluto, but in which terms smaller than e^2 and I^2 in the disturbing function are ignored. For the Koronis, Eos and Themis families, the errors introduced by this truncation are less than 5 percent (J. G. Williams, private communication, 1984).

TABLE 1: PROPER ORBITAL ELEMENTS OF FAMILIES

Family	a AU	e'	I' ± δI' deg	$(I'/\delta I')^{\frac{1}{2}}$
Koronis	2.875	0.049	2.12 ± 0.08	5.1
Eos	3.015	0.071	10.20 ± 0.28	6.0
Themis	3.136	0.152	1.42 ± 0.22	2.5

The forced eccentricity, e_f, can be further resolved into vectorial components given by

$$e_f \begin{matrix}\sin \\ \cos\end{matrix} \tilde{\omega}_f = \sum_{j=1}^{8} \sum_{\ell=1}^{10} \frac{M_{j\ell}[0,j]}{\dot{\tilde{\omega}}' - \dot{\nu}_\ell} \begin{matrix}\sin \\ \cos\end{matrix} (\dot{\nu}_\ell t + \nu_{0_\ell}) , \qquad (3)$$

where

$$\dot{\tilde{\omega}}' = \sum_{j=1}^{8} (0,j) , \qquad (4)$$

the (0,j) and the [0,j] are the Lagrange parentheses of the j^{th} planet, the $\dot{\nu}_\ell$ are the eigenfrequencies of the solar system associated with the motions of the pericenters of the planetary orbits and the $M_{j\ell}$ are coefficients in the expansion of the planetary eccentricities (Brouwer and Clemence, 1961). Similar expressions can be written for the forced inclination, I_f.

There are two important circumstances in which a single term or group of terms can dominate the double summation shown in equation (3). One occurs when an asteroid orbits close to a massive planet. As $a \to a_j$, where a and a_j are the semimajor axes of the asteroid and the j^{th} planet, respectively, both (0,j) and [0,j] increase as $[1 - (a/a_j)^2]^{-2}$.

https://doi.org/10.1017/S0252921100084980 Published online by Cambridge University Press

TABLE 2: FORCED ORBITAL ELEMENTS

Family	I_f deg	Ω_f deg	e_f	$\tilde{\omega}_f$ deg	$a(1-e') \pm ae_f$ AU
Koronis	1.16	96.1	0.037	6.2	2.73 ± 0.11
Eos	1.19	97.1	0.037	7.6	2.80 ± 0.11
Themis	1.22	97.8	0.038	8.7	2.66 ± 0.12

If $(0,j)$ is large and $\dot{\tilde{\omega}}' \gg \dot{\nu}_\ell$ for all ℓ, which is the case for asteroids orbiting close to Jupiter, then, as $a \to a_j$,

$$e_f \begin{matrix}\sin \\ \cos\end{matrix} \tilde{\omega}_f \to \frac{[0,j]}{(0,j)} e_j \begin{matrix}\sin \\ \cos\end{matrix} \tilde{\omega}_j , \tag{5}$$

$$= \frac{b_{3/2}^{(2)}(\alpha)}{b_{3/2}^{(1)}(\alpha)} e_j \begin{matrix}\sin \\ \cos\end{matrix} \tilde{\omega}_j , \tag{6}$$

where the $b_s^{(k)}(\alpha)$ are Laplace coefficients with $\alpha = a/a_j$ for $a < a_j$. Furthermore, as $a \to a_j$, $b_{3/2}^{(2)}(\alpha)/b_{3/2}^{(1)}(\alpha) \to 1$, so that $e_f \to e_j$ and $\tilde{\omega}_f \to \tilde{\omega}_j$. Similarly, $I_f \to I_j$ and $\Omega_f \to \Omega_j$; that is, the forced orbit locks onto and duplicates the orbit of the dominant planet. As seen in Figs. 2 and 3, this occurs for asteroidal orbits when $a \gtrsim 3$ AU.

If Jupiter were the only important influence on the asteroidal orbits, then e_f and $\tilde{\omega}_f$ (and I_f and Ω_f) would be poor indicators of distance, since they would vary little across the belt. However, resonant terms for which $\dot{\tilde{\omega}}' \approx \dot{\nu}_\ell$ (or $\dot{\Omega}' \approx \dot{\nu}_\ell$ in the analogous equations describing the motions of the nodes) can also dominate equation (3). Since three of these resonances occur in, or near, the main asteroid belt, the forced elements can be used to determine a. For small e and I, the $\dot{\nu}_{16} = \dot{\Omega}'$ and the $\dot{\nu}_6 = \dot{\tilde{\omega}}'$ resonances are located at 1.94 and 2.03 AU while the $\dot{\nu}_{10} = \dot{\tilde{\omega}}'$ resonance is located at 2.64 AU. The complete variations of e_f, $\tilde{\omega}_f$, I_f, and Ω_f across the main belt are shown in Figs. 2 and 3. For $a < 2.7$ AU, the forced orbital elements vary markedly with semimajor axis and thus, in the inner half of the asteroid belt, at least, they are good indicators of distance.

https://doi.org/10.1017/S0252921100084980 Published online by Cambridge University Press

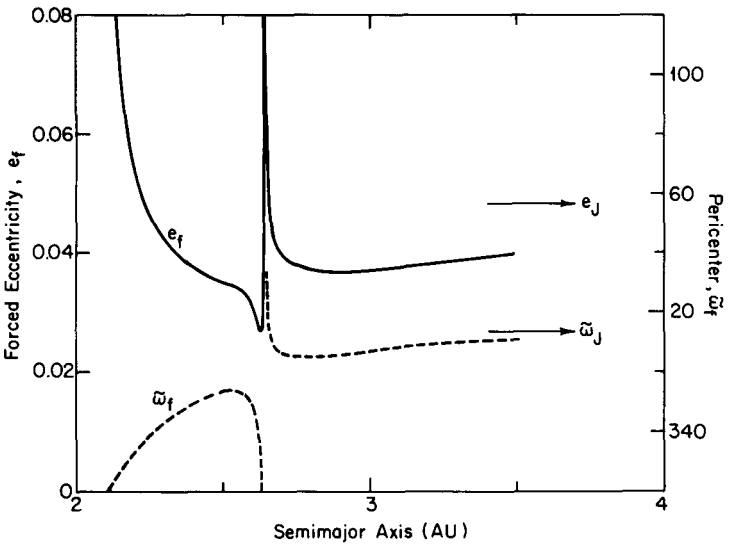

Fig. 2 Variation of the forced eccentricity e_f and the corresponding longitude of pericenter $\tilde{\omega}_f$ with semimajor axis in the main asteroid belt. The elements with subscript J are the present elements of Jupiter.

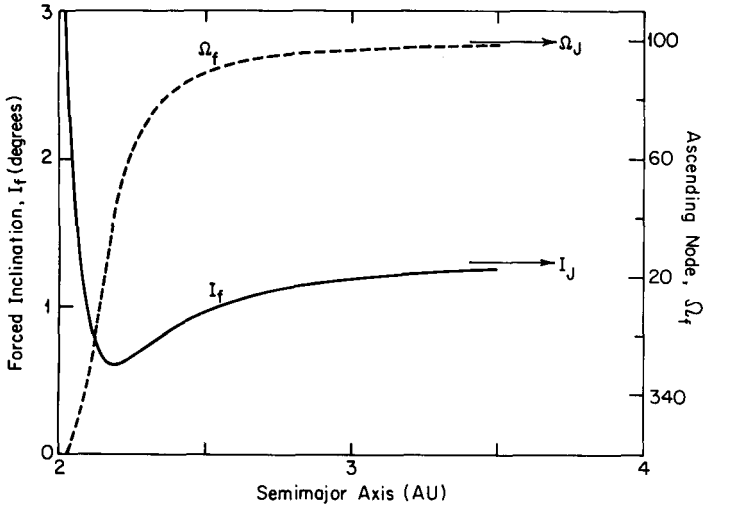

Fig. 3 Variation of the forced inclination I_f and the corresponding longitude of ascending node Ω_f with semimajor axis in the main asteroid belt. The elements with subscript J are the present elements of Jupiter.

https://doi.org/10.1017/S0252921100084980 Published online by Cambridge University Press

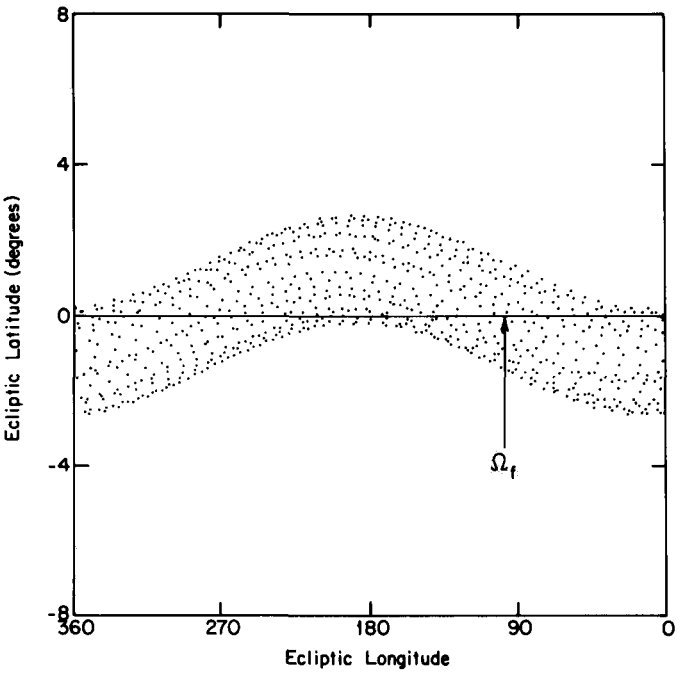

Fig. 4 Variation of ecliptic latitude with ecliptic longlitude, as measured in a sun-centered coordinate system, for the putative Themis dust band. The latitudinal width of the band is 2I' at all longitudes. The striations are an artifact of the small number of points used in the simulation and disappear as the number of points increases. (Figure copyright of Nature, Macmillan Journals Ltd.)

In closing this section, it should be mentioned that the above analysis is inadequate near resonances involving the mean motions of an asteroid and Jupiter, particularly the first-order and the lower-order resonances that dominate the orbital parameter space between the 2:1 resonance at 3.27 AU and the orbit of Jupiter (Dermott and Murray, 1983).

3. PARTICLE DISTRIBUTIONS

The existence of common forced inclinations and eccentricities gives rise to longitudinal variations in the latitude and the brightness of the bands that are diagnostic of their distances (Dermott et al., 1984). Geometrically, the effect of the forced inclination is to make all orbits with a particular value of semimajor axis precess about a common mean plane, whose inclination and ascending node are given by I_f and Ω_f, respectively. The peaks in the latitudinal distribution of an asteroidal family are symmetrically disposed with respect to this mean plane and, in a sun-centered coordinate system, form two

https://doi.org/10.1017/S0252921100084980 Published online by Cambridge University Press

parallel bands around the sky separated by 2I'. The appearance of the putative Themis dust band in a sun-centered ecliptic coordinate system is shown in Fig. 4. The sinusoidal variation of mean latitude with longitude has an amplitude I_f and the phase of the variation is determined by Ω_f. Variations in the apparent latitudinal separation of the bands as seen from the earth, corresponding to changes in telescope pointing, also give a method of determining the distances of the bands (Hauser et al., 1984). With this method, however, allowance must be made for the variation in apparent latitude corresponding to the changes in the distances of the bands associated with the forced eccentricity (q.v.).

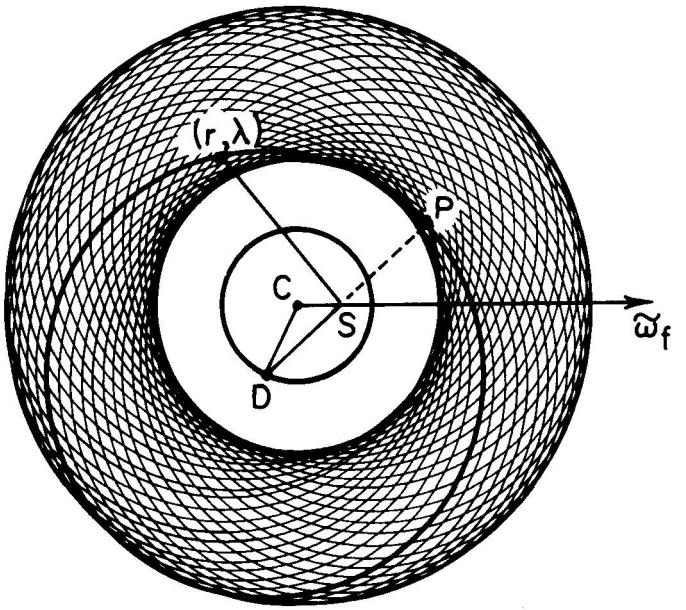

Fig. 5 Distribution of elliptical orbits. To order e, the figure is circularly symmetric about the point C which is displaced from the sun S by an amount ae_f in a direction opposite to that of $\tilde{\omega}_f$. The lines CS, DS and DC have lengths ae_f, ae and ae', respectively, and the triangle CDS is similar to the triangle CDS shown in Fig. 1. P is the pericenter of the highlighted orbit.

The effects of a forced eccentricity on the spatial distribution of an asteroidal family, or a dust band, are shown in Fig. 5. The distribution of the orbits depicted there can be understood from the properties of the vector diagram in Fig. 1. The distance of some point (r,λ) from the focus, S, in Fig. 5 varies, to lowest order in e, as

$$r = a[1 - e\cos(\lambda - \tilde{\omega}) + O(e^2)]. \qquad (7)$$

However, the distance r' of that same point from the center of its elliptical orbit, D, varies as

https://doi.org/10.1017/S0252921100084980 Published online by Cambridge University Press

$$r' = a[1 - \tfrac{1}{2}e^2\sin^2(\lambda - \tilde{\omega}) + O(e^3)] \ . \qquad (8)$$

Thus, to order e, an elliptical orbit can be represented by a circle of radius a centered on a point D which is displaced from its focus, S, by an amount ae in a direction opposite to that of its pericenter, P. Paradoxically, to order e, changing the eccentricity of an orbit does not result in a change in its shape: only its displacement from the focus changes. Since, in Fig. 1, the eccentricity vector e' rotates uniformly about C [cf. equations (1) and (2)], it follows that, in Fig. 5, the centers of the elliptical orbits are distributed uniformly on a circle of center C and radius ae' and that the orbits form an annulus of width 2ae' displaced by an amount ae_f in a direction opposite to that of $\tilde{\omega}_f$. To order e, the forced eccentricity e_f has no influence on either the shape, the size or the distribution of orbits within the annulus. It does, however, determine the displacement of the annulus from the common focus, S, and the longitudinal variation of the particle number density.

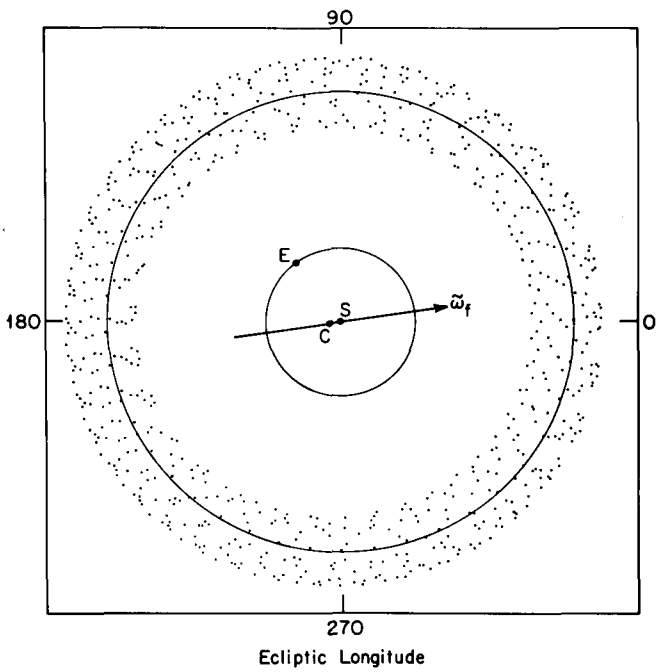

Fig. 6 A view of the putative Themis dust band in the ecliptic plane. The inner and the outer envelopes of the particle orbits are circularly symmetric about C (cf. Fig. 5). The radial width of the near-circular dust band is 2ae'. The solid circle within the dust band is centered on S and has a radius equal to the mean semimajor axis of the Themis family. The inner solid circle denotes the orbit of the earth E. (Figure copyright of Nature, MacMillan Journals Ltd.)

https://doi.org/10.1017/S0252921100084980 Published online by Cambridge University Press

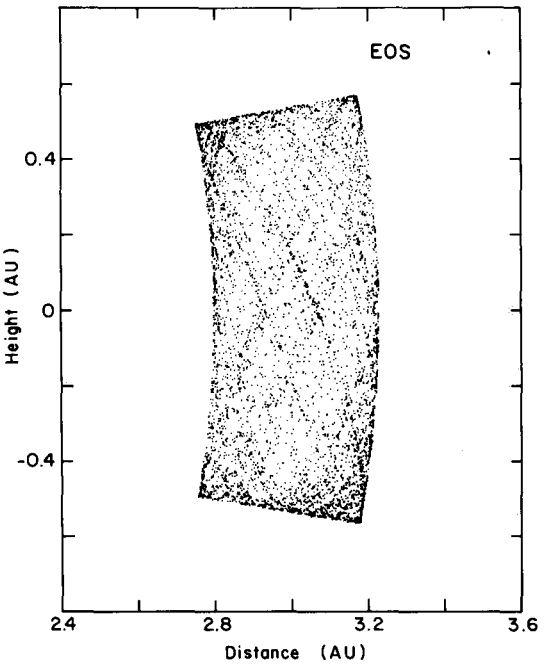

Fig. 7 A meridional cross-section of the putative Eos band. The particle number density is greatest at the corners of the distribution. Hence, from a point above the plane of the ecliptic an observer would see a pair of pericenter bands and a pair of apocenter bands.

The number of particles, $\delta N(\lambda,\tilde{\omega}')$, in a given section of the annulus on orbits with pericenters between $\tilde{\omega}'$ and $\tilde{\omega}' + \delta\tilde{\omega}'$, can be written

$$\delta N(\lambda,\tilde{\omega}') = \delta N_0 \delta N_p \ , \tag{9}$$

where δN_0 is the number of orbits in that section, as determined by $\delta\tilde{\omega}'$, and δN_p is the number of particles between λ and $\lambda + \delta\lambda$ on each orbit. Since $\tilde{\omega}'$ is distributed uniformly,

$$\delta N_0 = \frac{\delta\tilde{\omega}'}{2\pi} N_0 \ , \tag{10}$$

where N_0 is the total number of orbits in the annulus. From Kepler's law of areas,

$$\delta N_p \approx \frac{\delta\lambda}{2\pi}[1 - 2e \cos(\lambda - \tilde{\omega})]N_p \ , \tag{11}$$

https://doi.org/10.1017/S0252921100084980 Published online by Cambridge University Press

where N_p is the total number of particles on each orbit. Hence, the variation of particle number density with longitude, λ, is given by

$$N(\lambda)\delta\lambda = \frac{N\delta\lambda}{4\pi^2} \int_0^{2\pi} [1 - 2e \cos(\lambda - \tilde{\omega})] d\tilde{\omega}' \ , \qquad (12)$$

where N ($= N_0 N_p$) is the total number of particles. By using

$$\lambda - \tilde{\omega} = (\lambda - \tilde{\omega}_f) - (\tilde{\omega} - \tilde{\omega}_f) \ , \qquad (13)$$

to expand $\lambda - \tilde{\omega}$ in equation (12) and by eliminating $\tilde{\omega}$ through the use of

$$e \sin(\tilde{\omega} - \tilde{\omega}_f) = e' \sin(\tilde{\omega}' - \tilde{\omega}_f) \ , \qquad (14)$$

and

$$e \cos(\tilde{\omega} - \tilde{\omega}_f) = e' \cos(\tilde{\omega}' - \tilde{\omega}_f) + e_f \ , \qquad (15)$$

obtained from triangle CDS in either Fig. 1 or Fig. 5, equation (12) reduces to

$$N(\lambda)\delta\lambda = \frac{N\delta\lambda}{2\pi} [1 - 2e_f \cos(\lambda - \tilde{\omega}_f)] \ . \qquad (16)$$

Thus, the longitudinal variation of the particle number density is determined by e_f alone and is independent of e'. Two orthogonal views of typical particle distributions are shown in Figs. 6 and 7.

4. BRIGHTNESS VARIATIONS

Regardless of the source of the particles, longitudinal variations in brightness are predicted to exist in the IRAS data for two reasons. The particle number density is a minimum in the direction of $\tilde{\omega}_f$, but at $\lambda = \tilde{\omega}_f$ the particles are both closer to the earth's orbit and hotter. These latter effects more than compensate for the lower particle number density so that the dust bands are predicted to be brightest at pericenter (Dermott et al., 1984). The expected variations of brightness with ecliptic longitude, averaged over all latitudes, at the wavelengths that correspond to the four IRAS channels, are shown in Fig. 8. The phase of the longitudinal variation in brightness of each dust band is determined by $\tilde{\omega}_f$ and is therefore diagnostic of the dust band's semimajor axis, a, according to Fig. 2.

The relative amplitudes of the longitudinal variations in the four IRAS wavelength channels are determined by further properties of the dust grains, in particular, their albedos and radii. The particular calculation shown in Fig. 8 applies to the putative Themis band, but calculations for the Eos and the Koronis dust bands give almost identical results. For this heuristic model we have assumed (a) that

https://doi.org/10.1017/S0252921100084980 Published online by Cambridge University Press

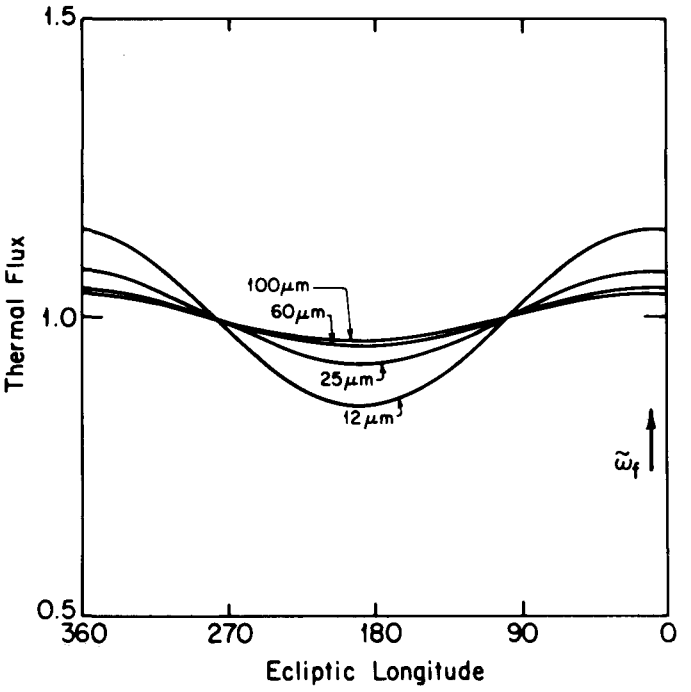

Fig. 8 Expected variation, with sun-centered ecliptic longitude, averaged over all latitudes, of the radiation received at the earth in the 12 μm, 25 μm, 60 μm, and 100 μm IRAS wavelength channels from dust particles associated with the Themis family. The arrow marks the longitude of perihelion of the forced eccentricity, $\tilde{\omega}_f$. (Figure copyright of Nature, MacMillan Journals Ltd.)

the radii of the dust particles are large (≫ the wavelengths of the IRAS observations), (b) that they have an emissivity of 0.9, a geometric albedo of 0.1 and a phase integral of 0.6, (c) that the earth's orbit is circular and (d) that the pointing direction of the IRAS telescope is tangential to the earth's orbit. The ecliptic longitude in Fig. 8 refers to the heliocentric longitude of the dust particles, rather than to their observed geocentric longitude, although the flux is that at the earth. The mean temperature of the dust particles associated with the Themis family is 160K. At this temperature, the Planck function peaks at a wavelength of 18 μm. The longitudinal variation in flux is strongest in the 12-μm channel because comparatively large changes in the thermal flux at wavelengths near 18 μm are produced by modest temperature changes.

Changes in the viewing aspect of the dust bands caused by longitudinal variations in their ecliptic latitude also result in longitudinal variations in brightness. A meridional cross section of a typical dust band is shown in Fig. 7. The harmonic oscillations of the

https://doi.org/10.1017/S0252921100084980 Published online by Cambridge University Press

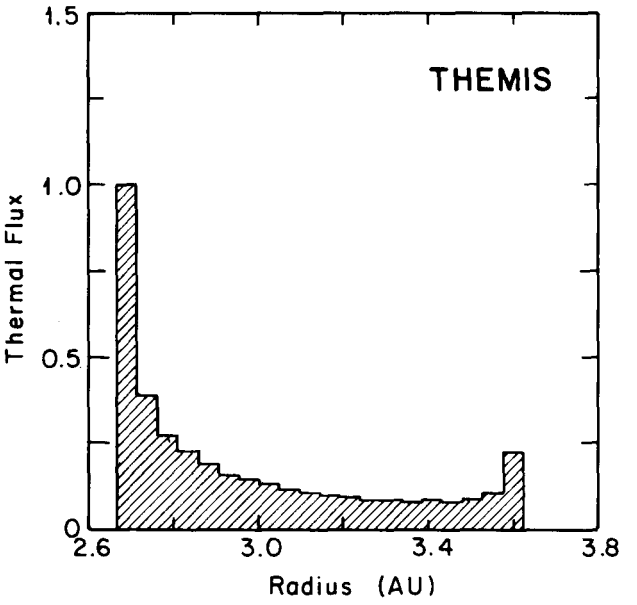

Fig. 9 The radial variation, averaged over all longitudes and latitudes, of the received radiation in the IRAS 12-μm channel, for the putative Themis dust band, as seen from its geometrical center, C. The inner edge of the band is four times as bright as the outer edge.

particles about their mean circular orbit result in a concentration of particles near the edges and, in particular, the corners of the cross section. From a viewpoint well above the plane of the ecliptic, an observer would see each of the two heliocentric bands split into a pair of bands, one band in each pair associated with the perihelia of the dust particle orbits and the other associated with their aphelia. The Voyager 1 spacecraft, which is at present leaving the solar system, may provide such a viewpoint (C. Porco, personal communication, 1984). These bands should also be sought in the data returned from the Pioneer integrated starlight experiment (Hong et al., 1985), which seems to find undulations in the zodiacal light brightness.

The perihelion and the aphelion bands, however, would not be equally bright. The expected radial variation, averaged over all longitudes and latitudes, of the thermal flux received in the IRAS 12-μm channel from the putative Themis dust band at its geometrical center, C, is shown in Fig. 9. The inner edge of the band is four times as bright as the outer edge and, thus, from a terrestrial viewpoint, we would expect the aphelia bands to be comparatively weak, particularly in the 12-μm channel. The difference between the perihelion and the aphelion bands is, however, less pronounced for the other families due to their smaller proper eccentricities.

https://doi.org/10.1017/S0252921100084980 Published online by Cambridge University Press

The heliocentric distance of the prominent perhelia band varies as

$$r = a[1 - e' - e_f \cos(\lambda - \tilde{\omega}_f)] \ . \qquad (17)$$

The mean distance of the perihelia bands associated with the Koronis, Eos, and Themis families is ~ 2.73 AU (see Table 2). This distance compares favorably with the distance of 2.7 ± 0.5 AU estimated from the color temperatures of the bands (Low et al., 1984) and with the distance of 2.5 AU derived from parallax measurements (Hauser et al., 1985). However, as we have already remarked, the latter estimate needs to be corrected for the variation in the distance of the perihelia band given by equation (17).

For an annulus like that shown in Fig. 7, an observer at the sun would only see two bands separated by $2I'$ (Dermott et al., 1984), since the aphelion and the perihelion bands would be superposed. The ratio of the brightness extremes, at a given longitude, seen by such an observer, that is, the ratio, R, of the brightness at the edge of the band to that its center, is determined by the resolution of the telescope (or the angle over which the data are binned), δI, and by the dispersion, $\delta I'$, in the proper inclinations of the dust particle orbits. R cannot exceed $\sim(I'/\delta I')^{\frac{1}{2}}$. However, if $\delta I' \ll \delta I$, then

$$R = (2I'/\delta I)^{\frac{1}{2}} \ . \qquad (18)$$

Maximum values of R, from a solar viewpoint, for the Koronis, Eos, and Themis families are listed in Table 1.

Because of the non-heliocentric vantage point of the IRAS telescope, the observed values of R will be significantly less than the above maxima; moreover, due to the forced inclinations of the bands and the resulting changes in the viewing geometry, they will vary with ecliptic longitude. We deduce from Fig. 4 that, at a heliocentric ecliptic longitude, λ, of $\Omega_f + 90°$, for an earth-bound telescope pointing in a direction radially away from the sun, R would be a minimum in the Northern band and a maximum in the Southern band, whereas, at $\lambda = \Omega_f - 90°$ the reverse would apply. Since the pointing direction of the IRAS telescope was predominantly in, or close to, a plane perpendicular to the direction of the sun, the above deductions do not strictly pertain to the IRAS data. However, for a telescope pointing plane fixed with respect to the direction of the sun, and for a fixed pointing sense within that plane, we expect that the band brightness will vary sinusoidally with ecliptic longitude and that there will be a phase shift of 180° between the brightness variations in the Northern and in the Southern bands.

The two sources of longitudinal variation in brightness that we have identified are, in principle, separable. The sum of the brightnesses in the Northern and in the Southern bands is determined by e_f and $\tilde{\omega}_f$ and is independent of I_f and Ω_f, whereas, for the ratio of

https://doi.org/10.1017/S0252921100084980 Published online by Cambridge University Press

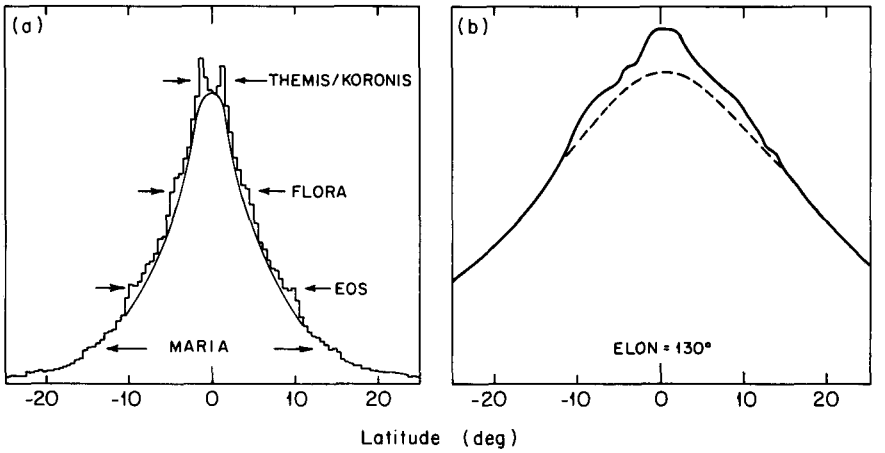

Fig. 10 A simulation of the the latitudinal distribution of dust particles associated with the ~ 2000 asteroids in the TRIAD file, (a), is compared with the IRAS flux data in the 60 μm wavelength channel (from Low et al., 1984), (b). In (a), latitude is measured with respect to the mean plane of the Eos family, whereas in (b) latitude is referred to the plane of the ecliptic. Deviations from the smooth curve in (a) are associated with the principal Hirayama families. In (b), ELON refers to the geocentric ecliptic longitude of the IRAS telescope pointing direction and the dashed curve represents the smooth zodiacal emission.

these brightnesses the opposite applies. All of these quantities are separately diagnostic of the bands' semimajor axes. Accurate predictions of R and its longitudinal variation for a given band, however, will require detailed modelling of the IRAS observations, beyond that attempted to date. The high-resolution IRAS data will be of particular interest, since R for this data will depend partly on the dispersion, $\delta I'$, in I', and partly on e'. Since $\delta I'$ for collision products is determined by the size of the parent body (collision products tend to disperse with relative velocities comparable to the escape velocity of the parent body), measurements of R should yield some information on the initial sizes of the dust particle sources.

5. PARTICLE SOURCES

Detailed analysis of the IRAS data should yield information on all the orbital elements of the dust particles and hence should disclose the source of the particles. Apart from the asteroid family model that we have discussed in detail above, and elsewhere (Dermott et al., 1984), the most plausible alternative model would involve the disintegration of one or more comets. In this case, however, the small-e and -I approximations would require some revision; nevertheless, our analytical approach should be equally suitable. In Fig. 10 we compare

https://doi.org/10.1017/S0252921100084980 Published online by Cambridge University Press

the IRAS flux data with the latitudinal distribution of dust particles associated with the known asteroidal orbits. It follows from this figure, and from a comparison of the relative volumes of the asteroids in the prominent families and those in the remainder of the belt, that, if the asteroid families provide the emitting area of the dust rings observed by IRAS, then the area of the entire asteroid belt must make a substantial contribution to the IRAS zodiacal signal.

This research was supported by grants from NASA and from NSF.

6. REFERENCES

Brouwer, D. and Clemence, G.M. Methods of Celestial Mechanics (Academic, New York, 1961).

Brouwer, D. and van Woerkom, A.J.J. (1950), Astr. Pap. U.S. Naval Obs. Naut. Almanac Off. Part II, 85-107.

Dermott, S. F., and Murray, C. D. (1983), "Nature of the Kirkwood gaps in the asteroid belt" Nature 301, 201-205.

Dermott, S. F., Nicholson, P. D., Burns, J. A., and Houck, J. R. (1984), "Origin of the solar system dust bands discovered by IRAS" Nature (in press).

Dohnanyi, J. S. (1976), "Sources of interplanetary dust: Asteroids" in Interplanetary Dust and Zodiacal Light (eds. Elsasser, H., and Fechtig, H.) 187-205 (Springer-Verlag, Berlin).

Hauser, M. G., Gautier, T. N., Good, J., and Low, F. J. (1985) "IRAS observations of interplanetary dust emission" (this conference).

Hong, F. F., Misconi, N. Y., Van Dijk, M.H.H., Weinberg, J. L., and Toller, G. N. (1985), "A search for small scale structure in the zodiacal light" (this conference).

Low, F. J., Beintema, D. A., Gautier, T. N., Gillet, F. C., Beichmann, C. A., Neugebauer, G., Young, E., Aumann, H. H., Boggess, N., Emerson, J. P., Habing, H. J., Hauser, M. G., Houck, J. R., Rowan-Robinson, M., Soifer, B. T., Walker, R. G., and Wesselius, P. R. (1984), "Infrared cirrus: New components of the extended infrared emission" Ap. J. 278, L19-L22.

Neugebauer, G., Beichmann, C. A., Soifer, B. T., Aumann, H. H., Chester, T. J., Gautier, T. N., Gillet, F. C., Hauser, M. G., Houck, J. R., Lonsdale, C. J., Low, F. J., and Young, E. (1984), "Early results from the Infrared Astronomical Satellite" Science 224, 14-21.